ARTICLE

SiCO-doped Carbon Fibers with Unique Dual Superhydrophilicity/Superoleophilicity and Ductile and Capacitance Properties

Ping Lu,[†] Qing Huang,[‡,§] Amiya Mukherjee,[‡] and You-Lo Hsieh*[,†]

Fiber and Polymer Science and Department of Chemical Engineering & Materials Science, University of California, Davis, California 95616, United States, and Ningbo Institute of Material Technology & Engineering, Chinese Academy of Sciences, Ningbo, China

ABSTRACT Silicon oxycarbide (SiCO) glass-doped carbon fibers with an average diameter of 163 nm were successfully synthesized by electrospinning polymer mixtures of preceramic precursor polyureasilazane (PUS) and carbon precursor polyacrylonitrile (PAN) into fibers then converting to ceramic/carbon hybrid via cross-linking, stabilization, and pyrolysis at temperatures up to 1000 °C. The transformation of PUS/PAN polymer precursors to SiCO/carbon structures was confirmed by EDS and FTIR. Both carbon and SiCO/carbon fibers were amorphous and slightly oxidized. Doping with SiCO enhanced the thermal stability of carbon fibers and acquired new ductile behavior in the SiCO/carbon fibers with significantly improved flexibility and breaking elongation. Furthermore, the SiCO/carbon fibers exhibited dual superhydrophilicity and superoleophilicity with water and decane absorbing capacities of 873 and 608 %, respectively. The cyclic voltammetry also showed that SiCO/carbon composite fibers possess better capacitor properties than carbon fibers.

KEYWORDS: silicon oxycarbide • carbon fiber • superhydrophilicity • superhydrophobicity • ductile capacitance

INTRODUCTION

Carbon fibers consist of more than 90 % of chemically bonded pure carbon (1, 2) and have remarkably high strength (3−7 GPa) and modulus (200−500 GPa) due to the highly anisotropic sheet-like graphite layers along the fiber axes (3−5). With its high strength-to-weight ratio and superior stiffness as well as other excellent engineering properties such as wear resistance, low expansion coefficient and relative flexibility, carbon fibers have been widely used to reinforce plastics in advanced composite structures for aerospace, defense, and industrial applications (6, 7).

Carbon fiber reinforced ceramic matrix composites are promising for applications requiring not only high strength, high fracture toughness, and low specific weight but also at ultrahigh temperatures (8, 9). More recently, fabricating silicon-containing CMCs from polysilanes, polysiloxanes, polycarbosilanes, and polysilazanes, the so-called polymer-derived ceramics (PDCs), has gained interest because of the advantages of their low processing temperatures, controllable ceramic compositions and neat-net-shapes (10). Carbon fiber reinforced silicon oxycarbide (SiCO) has been obtained through polymer-infiltration-pyrolysis method with improved mechanical property and thermal stability (11−14). Moreover, the excellent oxidation resistance, corrosion resistance, and high-temperature stability (up to 1500 °C) of the SiCO ceramic matrix help to inhibit oxidation of the incorporated carbon fibers at elevated temperatures (10, 15−25). However, to the best of our knowledge, SiCO-filled carbon fibers have not yet been reported in the published literature.

The objective of this study is to devise a method to incorporate ceramic compositions into the structure of carbon fibers and to investigate the resultant structure and properties. To obtain a carbon matrix with homogeneously distributed ceramic domains, we combined preceramic polyureasilazane (PUS) with polyacrylonitrile (PAN) carbon precursor before transforming into bi-component fibers. In this context, the SiCO ceramic precursor PUS was ideal because of its low viscosity and good solubility in various solvents (26), allowing mixing with PAN, the well-established carbon precursor with high carbon yield and chemical stability (27). The electrospinning technique that has demonstrated to be effective to fabricate uniform and submicrometer to nanometer ceramic and carbon fibers (27−29) was employed to process the PUS/PAN mixtures into fibers. The as-spun precursor composite fibers were then converted to SiCO/carbon composite fibers through cross-linking, stabilization, and carbonization processes by heating at temperatures up to 1000 °C in air and argon. The mechanical properties as well as surface wetting, structural morphologies, and electrochemical properties of the SiCO/carbon composite fibers were thoroughly investigated.

EXPERIMENTAL SECTION

Materials. Polyacrylonitrile (PAN) (M_w = 150 kDa) was purchased from Sigma-Aldrich Chemical Co. Inc. (Milwaukee, WI). KDT CERASET polyureasilazane (PUS) (KiON Defense

* To whom correspondence should be addressed. Tel.: +1 530 752 0843. E-mail: ylhsieh@ucdavis.edu.

Received for review September 24, 2010 and accepted November 18, 2010

† Fiber and Polymer Science, University of California.

‡ Department of Chemical Engineering & Materials Science, University of California.

§ Chinese Academy of Sciences.

DOI: 10.1021/am100918x

Published on Web 12/07/2010

Technologies, Inc.) was used as the preceramic precursor to prepare silicon oxycarbide (SiCO) glass. Acetone *N*,*N*-dimethylformamide (DMF) and ethanol, from EMD Chemicals, were used as received without further purification. All water used was purified by Milli-Q plus water purification system (Millipore Corporate, Billerica, MA).

Electrospinning of Composite Fibers. Preceramic polymer PUS and PAN mixed at 5/7 w/w PUS/PAN ratio were vigorously stirred for 24 h to achieve a 12 wt % total polymer concentration in DMF. The PUS/PAN mixture was loaded into a 20 mL syringe (National Scientific) fitted with a 23 gauge inner diameter flat metal needle (BD Medical Franklin Lakes, NJ) and fed at 1 mL/h with a syringe pump (KDS 200, KD Scientific, USA). Electrospinning was performed by applying 15 kV voltage using a DC power supply (ES 30−0.1 P, Gamma High Voltage Research Inc., Ormond Beach, FL) to the metal needle at 23.9 °C and 34% relative humidity. The charged jet sprayed into fine fibers that were collected on a perpendicularly standing aluminum plate (30 cm ×30 cm) placed 25 cm from the tip of the needle. The electrospun PUS/PAN fibrous membrane was vacuum-dried at ambient temperature for 24 h. As comparison, pure PAN fibers were also electrospun from a 7 wt % PAN DMF solution under the same conditions described above.

Formation of SiCO/Carbon Fibers. The as-spun PUS/PAN (or PAN) fibrous mats were rolled around on a quartz tube to maintain certain tension and to prevent shrinkage and pyrolyzed in air and argon by a three-step process using a tube furnace (Mini-Mite, Lindberg/Blue). The samples were first heated at 5 °C/min to 250 °C in air and incubated for 60 min to cross-link and stabilize the fiber structures. The atmosphere was then changed to argon and the temperature was increased at 1 °C/min from 250 to 750 °C and held at the temperature for 1 h to completely remove the organics in PUS and PAN. Finally, the temperature was rapidly increased to 1000 °C at a ramp rate of 10 °C/min and held for another 1 h to mineralize the sample to so-called pyrolyzed fibers.

Characterization. The microstructures and surface morphologies of the products were examined by a scanning electron microscope (SEM) (XL 30-SFEG, FEI/Philips, USA). The fiber diameter and size distribution were evaluated by an image analyzer (analySIS FIVE, Soft Imaging System). The chemical composition and element distribution of the samples were mapped by the energy-dispersive X-ray spectrometer (EDS) in conjunction with the SEM. The crystalline phases present in the powder samples were determined by X-ray diffraction (XRD) (Scintag XDS 2000 powder diffractometer) at 45 kV and 40 mA from 5° to 80° with a Ni-filtered Cu $K\alpha_1$ radiation ($\lambda = 1.542$ Å). The Fourier transform infrared (FTIR) spectra were collected from 4000 to 400 cm^{-1} at 128 scans with a 4 cm^{-1} resolution by a Nicolet 6700 spectrometer (Thermo Fisher Scientific, USA). The thermal behaviors of PAN and PUS/PAN composite fibers were recorded by heating in N_2 at 10 °C/min from 30 to 1000 °C with a thermogravimetric analyzer (TGA-50, Shimadzu, Japan). The surface area, pore volume, and pore size distribution of as-spun PAN, PUS/PAN fibers, and their corresponding carbon and SiCO/carbon composite fibrous mats were derived from N_2 adsorption−desorption isotherms at 77 K by the Brunauer−Emmett−Teller (BET) equation in a relative pressure range of $p/p_o = 0.06-0.20$ and the Barrett−Joyner−Halenda (BJH) method from the adsorption branch of the isotherms using a surface area and porosity analyzer (ASAP 2020, Micromeritics, USA). The surface wetting and dynamic absorption were measured on 5 mm × 25.4 mm samples vertically placed with the 5 mm edge immersed in water and decane using a tensiometer (K14, KRUSS, USA). The tensile properties of the carbon and SiCO/carbon fibrous mats were measured using an Instron tensile tester (5566, Illinois Tool Works Inc., USA) equipped with a ±10 N load cell (0.00001 N resolution) and rubber-coated grips (1 in wide) at a 10 mm gauge length and a 5 mm/min cross-head speed at 21 °C and 65% relative humidity. The specimen were cut along the vertical direction to the rolling direction of the electrospun fibrous membranes to a 5 mm wide and 20 mm long size. The thicknesses and weight of the mats were measured by a thickness tester (Custom Scientific Instruments, Inc., Whippany, NJ) and a balance with accuracy to 0.01 mg (AUW220D, Shimadzu), respectively. For each fibrous mat, ten specimens within similar (±10%) thickness (∼0.1 mm) and weight (∼ 2 mg) or an apparent density (∼0.2 mg/mm^3) were used for tensile measurements. The Young's modulus of the samples is derived from the slope of the initial linear part of the stress−strain curves. The flexibilities or antifolding of the mats were examined by a recovery tester following a standard method. Briefly, fibrous mats were cut to 15 mm × 40 mm and placed between the leaves of the specimen holder with one end directly under the 18 mm mark. A load of 500 g was applied gently for 5 min. The electrochemical properties of carbon and SiCO/carbon fibrous mats were studied in 6 M aqueous KOH solution by a test cell of a capacitor with 1 V working potential and a cellulose filter paper was inserted between the two electrodes to be used as a separator in the electrolyte. Cyclic voltammetry (CV) of the cell was performed in the 0−1 V potential range by varying the scan rate from 50 to 1000 mV s^{-1} on a potentiostat/galvanostat (EG&G Princeton Applied Research, model 263A).

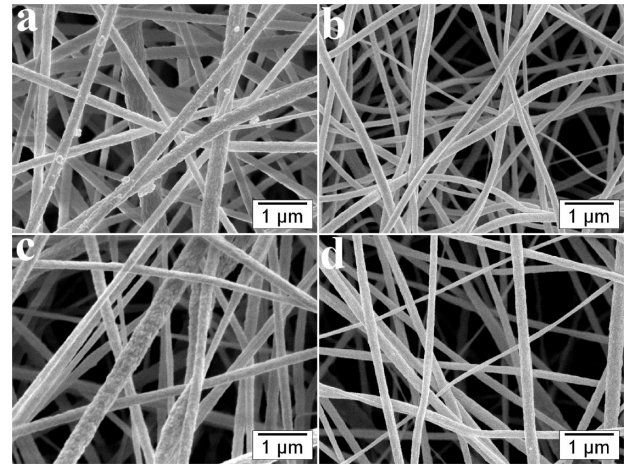

FIGURE 1. SEM images of the as-spun (a) PAN and (c) PUS/PAN fibers and their corresponding pyrolyzed (b) carbon and (d) SiCO/carbon composite fibers.

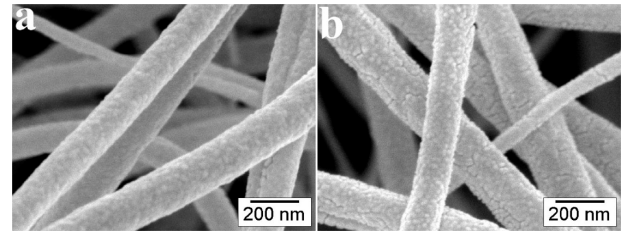

FIGURE 2. High-resolution SEM images showing the surface morphologies of (a) carbon and (b) SiCO/carbon composite fibers.

RESULTS AND DISCUSSION

Morphologies of As-Spun PAN and PUS/PAN and Their Pyrolyzed Fibers. Three dimensional nanofibrous mats of as-spun and carbonized PAN and PUS/PAN appear similar with random orientation (Figure 1) and rough surfaces (Figure 2). Upon pyrolysis, both fibers reduced significantly in diameters (Figure 3). Although the addition of PUS did not affect the general morphology or sizes of the

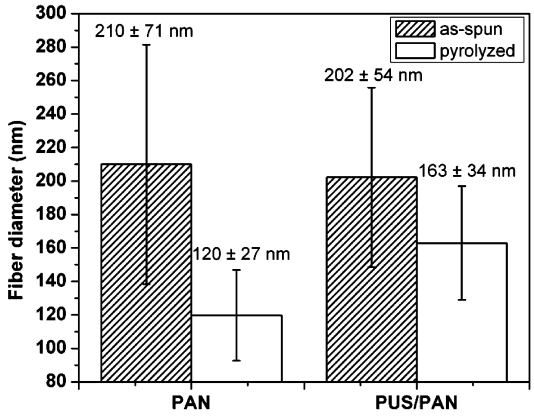

FIGURE 3. Diameters of the as-spun PAN, PUS/PAN, and their corresponding pyrolyzed fibers.

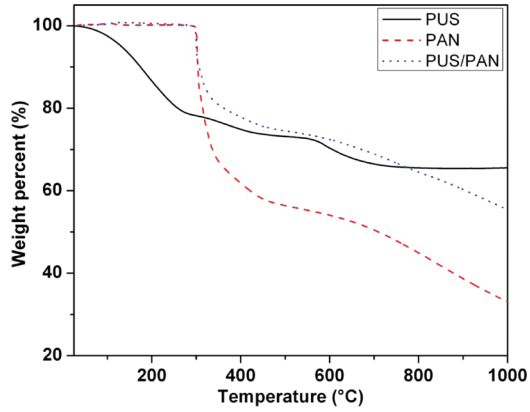

FIGURE 4. Thermal behaviors of crude PUS as well as as-spun PAN and PUS/PAN heated from room temperature to 1000 °C in N_2.

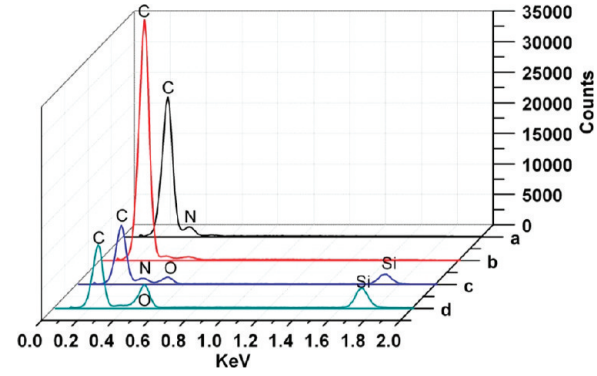

FIGURE 5. EDS spectra showing the compositions of as-spun (a) PAN and (c) PUS/PAN and (b, d) their corresponding pyrolyzed products.

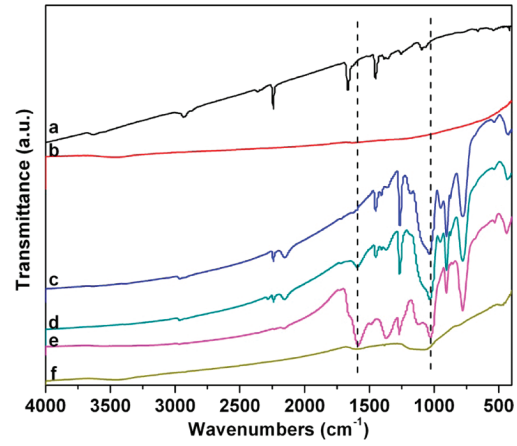

FIGURE 6. FTIR spectra of (a) as-spun PAN fibers, (b) PAN fibers pyrolyzed at 1000 °C, (c) as-spun PUS/PAN, and the corresponding samples pyrolyzed at (d) 200 °C, (e) 300 °C, and (f) 1000 °C.

as-pun fibers, it improved fiber size uniformity and retained more of the fiber dimension following the removal of the organic compositions and the side group condensation from pyrolysis under tension. Also the SiCO/carbon fibers remained straight as in the as-spun whereas some carbon fibers appeared curved. The better dimensional retention of SiCO/carbon fibers can be attributed to the cross-linking of PUS at low temperature (200−250 °C) and the better thermal stability of the resultant SiCO phase inside the fibers. The high-resolution SEM images in Figure 2 show carbon fibers with a relatively uniform surface morphology as opposed to the grainier and more cracking surfaces of SiCO/carbon fibers, possibly ascribed to the releasing of volatiles from PUS in the structural transition process.

Chemical and Physical Structures of the Fibers. The conversion of preceramic polymer PUS to SiCO generally occurs in three stages as evidenced by the TGA curve shown in Figure 4. The most significant mass loss is the initial 21.3% associated with moisture loss and cross-linking of the PUS side groups below 300 °C. Further condensation of the side groups and decomposition of the polymer framework were observed in the 300−600 °C temperature range and the final redistribution reaction and mineralization occurred at 600−1000 °C, each losing a few more percentage of mass, and leading to the formation of SiCO with a total 34.4% mass loss. Carbonization of PAN, on the other hand, showed only 33.1% mass retention, about half of its carbon content. However, the addition of PUS into PAN seems not to alter the trend of the TGA curve of PAN. Based on the 5/7 mass ratio of PUS/PAN as well as the observed mass loss for PUS and PAN individually, the additive mass loss for this composition would be 60.4%, much higher than the measured value of 44.6%. The higher solid residues in the pyrolyzed PUS/PAN composite indicate likely interactions between the decomposition reactions of PUS and PAN.

The effect of pyrolysis was clear from the disappearance of nitrogen and intensified carbon in the EDS spectra of the pyrolyzed products from both PAN and PUS/PAN (Figure 5). Oxidation was also evident in both cases. The FTIR spectra further confirmed the successful transformations of PAN to carbon structure as well as PUS/PAN to SiCO/carbon (Figure 6). All characteristic peaks of PAN at 2936, 1450 (CH, CH_2), and 2243 cm^{-1} (C≡N) (30, 31) disappeared after heating to 1000 °C (curve a), suggesting the successful removal of organic groups in the precursor PAN. The cross-linking and stabilization reactions of PUS/PAN composite fibers were evident by the decreased peak intensities of nitrile (CN) at 1450 cm^{-1} and Si−O at 1030 cm^{-1} as well as the advent of the conjugated C═C peak at 1582 cm^{-1} that intensified with heating to 200 (curve d) and 300 °C (curve e) (22, 32). The transition at approximately 300 °C between stabilization and further decomposition, with the exhibited structural changes in the spectra, agreed well with the significant initial weight loss in the TGA. In the final pyrolyzed product of PUS/

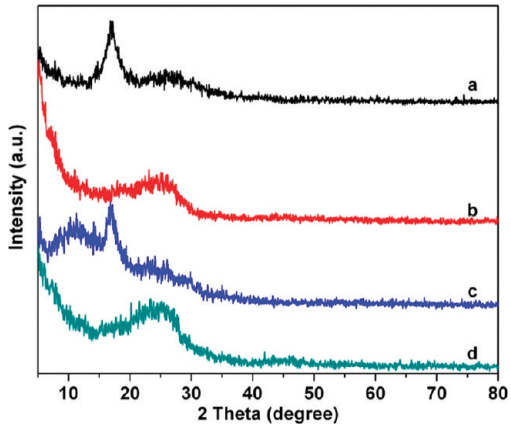

FIGURE 7. XRD patterns of (a) as-spun PAN, (b) carbon, (c) as-spun PUS/PAN, and (d) SiCO/carbon composite fibers.

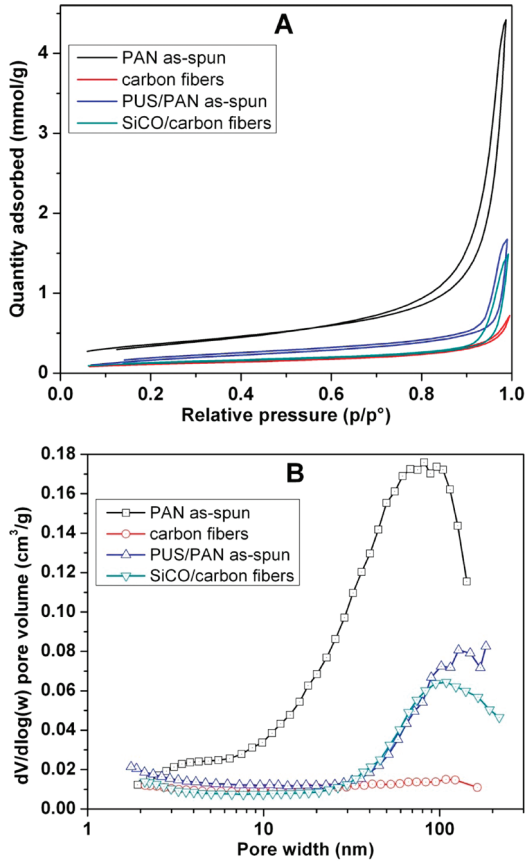

FIGURE 8. Pore characteristics of as-spun PAN, carbon, as-spun PUS/PAN, and SiCO/carbon fibers: (A) nitrogen adsorption−desorption isotherms at 77 K, (B) pore size distribution calculated from the adsorption branch of the isotherms by BJH method.

PAN, a broad peak centered at around 1065 cm^{-1} accompanied by a weak peak at 460 cm^{-1}, assigned to Si−O−Si stretching, and a shoulder peak at 816 cm^{-1} of Si−C as well as the conjugated C═C in graphite are present in the spectra (curve f), corroborating the formation of SiCO/carbon composite structure instead of a mixture of SiO_2 and carbon. The XRD patterns also disclose the successfully structural conversion in the samples (Figure 7). The strong diffraction peak at $2\theta = 17°$ for the as-spun PAN and PUS/PAN fibers can be assigned to 200 plane of PAN (28). The patterns of the carbon fibers (curve b) and SiCO/carbon fibers (curve d) reveal only broad amorphous peaks at 2θ around 25°, confirming both carbon and SiCO/carbon to be amorphous.

Table 1. BET Surface Areas and Pore Volumes of the Samples

	PAN as-spun	carbon fibers	PUS/PAN as-spun	SiCO/carbon fibers
BET surface area (m^2/g)	29.29	9.14	15.18	10.26
pore volume (cm^3/g)[a]	0.1544	0.0256	0.0588	0.0523

[a] Between 1.7 and 300 nm and from adsorption branch of the isotherms calculated by BJH method.

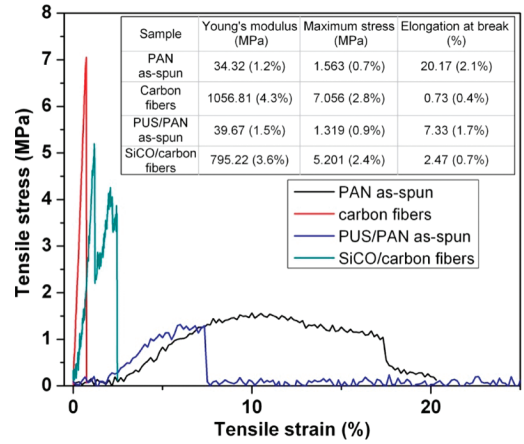

FIGURE 9. Mechanical properties of PAN, carbon, PUS/PAN, and SiCO/carbon fibrous membranes. All four samples were tested on at least 10 specimens each and the stress−strain curves shown here are representative and repeatable for at least 3 times. The data in the parentheses in the inset table are the variation coefficients of all specimens measured.

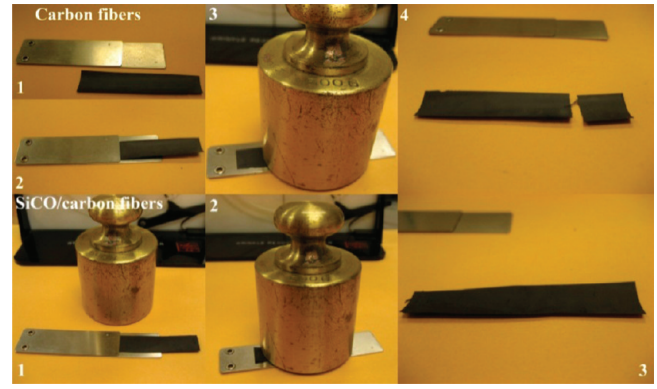

FIGURE 10. Flexibility or antifolding of the carbon (top) and SiCO/carbon (bottom) fibrous mats.

The surface areas and porosities of the as-spun PAN and PUS/PAN fibers as well as the amorphous carbon and SiCO/carbon fibers were measured by nitrogen adsorption−desorption at 77 K (Figure 8). The nitrogen adsorption−desorption isotherms of the as-spun and pyrolyzed samples are all type IV (Figure 8). The H3 hysteresis loops imply the slit-shaped pores in the fibers (Figure 8A). The loop positions of the isotherms are all present at the high relative pressures (p/p_o), pointing out the large pore sizes in these samples, consistent with the results from pore size distribution cal-

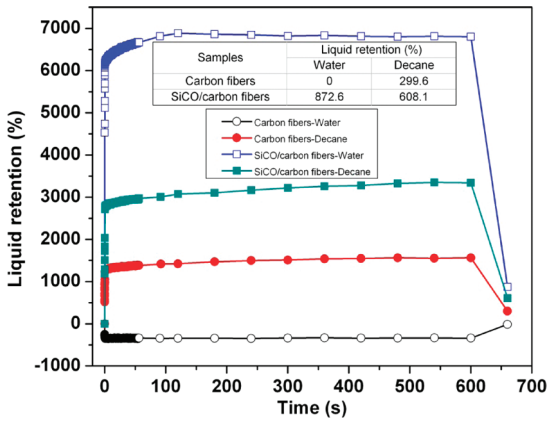

FIGURE 11. Dynamic absorption curves and liquid absorption (after leaving liquids) of fibrous mats in water and decane (liquid absorption was calculated as the mass ratio of the absorbed liquid over the sample).

culated from the adsorption branch of the isotherms by Barrett–Joyner–Halenda (BJH) method (Figure 8B). Carbon fibers have a wide pore size distribution that ranges from 1.7 to 100 nm, whereas the as-spun PAN fibers have a narrower one from 60–100 nm. Moreover, the Brunauer–Emmett–Teller (BET) surface areas and pore volumes were significantly reduced, from 29.29 m^2/g and 0.1544 cm^3/g for PAN fibers to 9.14 m^2/g and 0.0256 cm^3/g for carbon fibers, respectively (Table 1). These changes are likely due to the reduced fiber diameters and the resultant collapse and redistribution of pores in the fibers from pyrolysis. The pore size also exhibited a similar reduction from 135 nm for as-spun PUS/PAN fibers to 100 nm for the pyrolyzed SiCO/carbon fibers. It is likely that the smaller shrinkage in the transformation of PUS to SiCO and the better thermal stability of SiCO prevented the collapse of macropores into mesopores or micropores. This is also consistent with the smaller decreases in BET surface areas from 15.18 m^2/g of PAN/PUS to 10.26 m^2/g of SiCO/carbon as well as pore volumes from 0.0588 to 0.0523 cm^3/g. However, it should be noted that the density increases from PAN and PUS to carbon and SiCO could also play an important role in the decreased BET surface areas and pore volumes in addition to the changes in physical structures of the fibers.

Mechanical, Surface, and Electrochemical Properties. In lieu of the difficult single fiber tensile strength and elongation measurement by AFM (28), the gross mechanical properties of fibrous mats were measured. Typical stress–strain tensile properties of the fibrous mats are present in Figure 9 and the calculations are shown in the inset table. The as-spun PAN nanofibrous mats exhibited characteristic mechanical properties of nonwoven electrospun polymer sheet with low tensile strength (1.563 MPa) and modulus (34.32 MPa) but relatively high elongation (20.2%). Doping with PUS increased the modulus slightly to 39.67 MPa while decreasing the strength and elongation at break to 1.319 MPa and 7.33%, respectively. The carbon fibers possessed the highest mechanical strength among the four with 1057 MPa modulus and 7.056 MPa strength but the lowest elongation at break of 0.73%. The SiCO-doped carbon fibers had 3.4 times improved elongation (2.5%) with about 25%

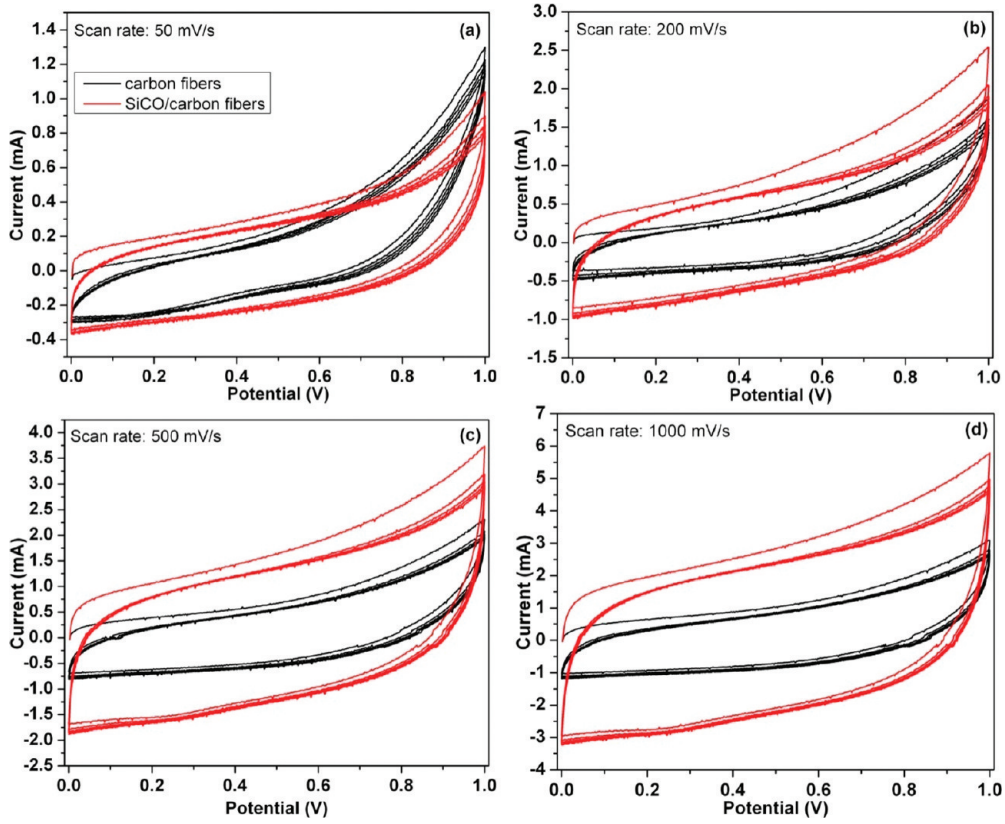

FIGURE 12. Cyclic voltammograms of an assembled capacitor using the as-prepared carbon nanofibrous mat and SiCO/carbon nanofibrous mat as electrodes under scan rates of (a) 50, (b) 200, (c) 500, and (d) 1000 mV/s.

reduced modulus (795.2 MPa) and strength (5.201 MPa). To measure the flexibility of the samples, another important property in addition to the mechanical strength, a simple method was designed to observe the capacity of the sample to recover from being folded under a 500 g load for 5 min (Figure 10). The carbon nanofibrous mat broken into two parts, whereas SiCO/carbon nanofibrous mat returned fully to its original shape without leaving any wrinkles, demonstrating remarkably enhanced structural flexibility and recovery capability.

The wetting and absorption properties measured in water and oil (here is decane) showed the carbon fibrous mat to be superhydrophobic, by displaying negative wetting force in contact with water (>90° contact angle) and a 0% water absorption after leaving water (Figure 11). The SiCO/carbon fibrous mat, on the other hand, exhibited superhydrophilicity with an 8.726-fold water absorption as opposed to zero of the carbon fibrous mat. Moreover, the SiCO/carbon fibers also demonstrated superoleophilicity, absorbing 6.081-fold decane by mass compared to 2.996-fold for carbon fibers. The difference in water and decane absorption of the SiCO/carbon fibrous mat reflects essentially the different liquid densities, i.e., 1 and 0.73 g/cm^3. Although carbon fibers are hydrophobic or oleophilic, the SiCO/carbon fibers possess the unique dual properties of superhydrophilicity as well as superoleophilicity.

The electrochemical properties of the as-prepared carbon and SiCO/carbon nanofibrous mats were investigated by cyclic voltammetry in a 6 M aqueous KOH solution acting as the electrolyte. Figure 12 shows the cyclic voltammograms (CVs) of the assembled capacitor using the carbon and SiCO/carbon fibrous mats as the electrodes. The CVs were recorded in the potential range of 0−1 V at 50, 200, 500, and 1000 mV/s scan rates. It is well-known that the CVs for an ideal double-layer capacitor should be in the shape of a perfect rectangle. Although the CVs of SiCO/carbon mat are not in perfect rectangular shapes at these four scan rates, they are relatively rectangular and are far more satisfactory than those distorted CVs of carbon mat, revealing well developed capacitance properties after doping carbon with SiCO glasses. Furthermore, no visible redox peaks were observed in the scan range, proving the chemical stability of the SiCO/carbon fibers.

CONCLUSIONS

In summary, carbon fibers and SiCO/carbon composite fibers with average diameters of 120 and 163 nm, respectively, were successfully fabricated by electrospinning the 7 wt % PAN and 5/7 wt % PUS/PAN in DMF, respectively, followed by cross-linking, stabilization and carbonization at temperatures up to 1000 °C. The carbon and SiCO/carbon structures from pyrolyzing PAN and PUS/PAN precursor composite fibers were confirmed by FTIR in the disappearance of the CH, CH_2 (2936, 1450 cm^{-1}), and C≡N (2243 cm^{-1}) characteristic peaks in PAN and the appearance of Si−O−Si and Si−C stretching as well as the conjugated C=C graphite structure. Both the carbon and SiCO/carbon composite fibers are amorphous as shown by XRD with slight oxidation as evident by EDS. The surface areas and pore volumes for the SiCO/carbon fibers are 10.26 m^2/g and 0.0523 cm^3/g, respectively, slightly higher surface area and nearly double pore volume than the carbon fibers (9.14 m^2/g and 0.0256 cm^3/g). The SiCO/carbon fibers have 26% lower tensile strength, but 3.4 times higher elongation at break than the carbon fibers. Most significantly is the remarkably improved flexibility of the SiCO/carbon fibers that was demonstrated by a full recovery without fracturing or even any crease from folding at 180° under a 500 g load for 5 min. Furthermore, the SiCO/carbon fibers exhibited dual superhydrophilicity (absorbing 873% water) and superoleophilicity (608% decane absorption). The electrochemical property by cyclic voltammetry shows that SiCO/carbon fibers possess better capacitance behaviors than carbon fibers. These unique mechanical and physical characteristics of the SiCO/carbon fibers show them to be a promising candidate for a broad range of high temperature applications, such as catalyst supporting material, protective coating, flexible electronics, etc.

Acknowledgment. This research was made possible by funding from the U.S. National Science Foundation (Grant CMMI #0700272) and National Textile Center (Project M10-CD02) as well as the Jastro-Shields Graduate Research Award and Summer Graduate Researcher Award from the University of California, Davis.

REFERENCES AND NOTES

(1) Donnet, J.-B. *Carbon Fibers*, 3rd ed.; Marcel Dekker: New York, 1998.
(2) Morgan, P. *Carbon Fibers and Their Composites*; Taylor & Francis: Boca Raton, FL, 2005.
(3) Liu, J.; Yue, Z. R.; Fong, H. *Small* **2009**, *5*, 536–542.
(4) Bunsell, A. R.; Renard, J. *Fundamentals of Fibre Reinforced Composite Materials*; Institute of Physics: Bristol, U.K., 2005.
(5) Buckley, J. D.; Edie, D. D. *Carbon−Carbon Materials and Composites*; Noyes Publications: Park Ridge, NJ, 1993; pp xiii.
(6) Chung, D. D. L. *Carbon Fiber Composites*. Butterworth-Heinemann: Boston, 1994; pp x.
(7) Fitzer, E.; Manocha, L. M. *Carbon Reinforcements and Carbon /Carbon Composites*; Springer-Verlag: Berlin, 1998.
(8) Wang, C.; Zhu, Z.; Hou, X.; Li, H. *Carbon* **2000**, *38*, 1821–1824.
(9) Wilshire, B.; Carreno, F. *J. Eur. Ceram. Soc.* **2000**, *20*, 463–472.
(10) Li, Y. L.; Fan, H.; Su, D.; Fasel, C.; Riedel, R. *J. Am. Ceram. Soc.* **2009**, *92*, 2175–2181.
(11) Ma, Q. S.; Chen, Z. H.; Zheng, W. W.; Hu, H. F. *Ceram. Int.* **2005**, *31*, 305–314.
(12) Wang, S.; Chen, Z. H.; Ma, Q. S.; Hu, H. F.; Zheng, W. W. *Mater. Sci. Eng., A* **2005**, *407*, 245–249.
(13) Ma, Q. S.; Chen, Z. H.; Zheng, W. W.; Hu, H. F. *J. Mater. Sci.* **2005**, *40*, 361–365.
(14) Shibuya, M.; Sakurai, M.; Takahashi, T. *Compos. Sci. Technol.* **2007**, *67*, 3338–3344.
(15) Manocha, L. M.; Manocha, S.; Patel, K. B.; Glogar, P. *Carbon* **2000**, *38*, 1481–1491.
(16) Ma, Q. S.; Chen, Z. H.; Zheng, W. W.; Hu, H. F. *J. Mater. Sci.* **2004**, *39*, 4901–4902.
(17) Pina, S. R. D. O.; Pardini, L. C.; Yoshida, I. V. P. *J. Mater. Sci.* **2007**, *42*, 4245–4253.
(18) Guo, H.; Huang, Y. D.; Liu, L.; Xu, L. W. *Mater. Des.* **2009**, *30*, 4498–4501.
(19) Pena-Alonso, R.; Soraru, G. D.; Raj, R. *J. Am. Ceram. Soc.* **2006**, *89*, 2473–2480.
(20) Pena-Alonso, R.; Mariotto, G.; Gervais, C.; Babonneau, F.; Soraru, G. D. *Chem. Mater.* **2007**, *19*, 5694–5702.
(21) Kleebe, H. J.; Blum, Y. D. *J. Eur. Ceram. Soc.* **2008**, *28*, 1037–1042.

(22) Pashchanka, M.; Engstler, J.; Schneider, J. J.; Siozios, V.; Fasel, C.; Hauser, R.; Kinski, I.; Riedel, R.; Lauterbach, S.; Kleebe, H. J.; Flege, S.; Ensinger, W. *Eur. J. Inorg. Chem.* **2009**, 3496–3506.
(23) Kroll, P. *J. Mater. Chem.* **2003**, *13*, 1657–1668.
(24) Colombo, P.; Hellmann, J. R.; Shelleman, D. L. *J. Am. Ceram. Soc.* **2002**, *85*, 2306–2312.
(25) Soraru, G. D.; Pederiva, L.; Latournerie, M.; Raj, R. *J. Am. Ceram. Soc.* **2002**, *85*, 2181–2187.
(26) Lu, P.; Huang, Q.; Jiang, D.; Ding, B.; Hsieh, Y.-L.; Ovid'ko, I. A.; Mukherjee, A. *J. Am. Ceram. Soc.* **2009**, *92*, 2583–2589.
(27) Kim, C.; Ngoc, B. T. N.; Yang, K. S.; Kojima, M.; Kim, Y. A.; Kim, Y. J.; Endo, M.; Yang, S. C. *Adv. Mater.* **2007**, *19*, 2341–2346.
(28) Hou, H. Q.; Ge, J. J.; Zeng, J.; Li, Q.; Reneker, D. H.; Greiner, A.; Cheng, S. Z. D. *Chem. Mater.* **2005**, *17*, 967–973.
(29) Chakrabarti, K.; Nambissan, P. M. G.; Mukherjee, C. D.; Bardhan, K. K.; Kim, C.; Yang, K. S. *Carbon* **2006**, *44*, 948–953.
(30) Ji, L. W.; Medford, A. J.; Zhang, X. W. *Polymer* **2009**, *50*, 605–612.
(31) Zhang, D.; Karki, A. B.; Rutman, D.; Young, D. R.; Wang, A.; Cocke, D.; Ho, T. H.; Guo, Z. H. *Polymer* **2009**, *50*, 4189—4198.
(32) Zhang, W. X.; Wang, Y. Z.; Sun, C. F. *J. Polym. Res.* **2007**, *14*, 467–474.

AM100918X